Two-Dimensional Tetragonal TiC Monolayer Sheet and Nanoribbons

Zhuhua Zhang,*[†,‡] Xiaofei Liu,[†] Boris I. Yakobson,[‡] and Wanlin Guo*[†]

[†]State Key Laboratory of Mechanics and Control of Mechanical Structures, Key Laboratory of Intelligent Nano Materials and Devices of MoE and Institute of Nano Science, Nanjing University of Aeronautics and Astronautics, Nanjing 210016, China

[‡]Department of Mechanical Engineering and Materials Science, Rice University, Houston, Texas 77005, United States

Ⓢ *Supporting Information*

ABSTRACT: We report a two-dimensional tetragonal Titanium Carbide (TiC) monolayer sheet with distinguished structure and properties based on comprehensive first-principles calculations. The TiC sheet exhibits a novel zigzag-shaped buckling structure with all atoms being quasiplanar tetracoordinate, as favored by strong in-plane C2p−Ti3d bonding and synergetic out-of-plane electronic delocalization. This unique structure endows the sheet with high kinetic stability and anisotropic mechanical properties. Moreover, the TiC sheet displays orientation-dependent electronic properties derived from its special rectangular symmetry, with indirect band gap of ∼0.2 eV and substantial ferromagnetism along its edges, thus promising for wide applications in nanoelectronics.

Figure 1. Structure of the t-TiC sheet. (a) Atomic structure of sheet with two basic vectors **a** and **b**; dashed rectangle marks sheet's primitive cell. (b) Isosurface plots (0.01 e/Å^3) of deformation electronic density. Charge accumulation and depletion regions are in yellow and red, respectively.

The fantastic properties of graphene, an allotrope of carbon consisting of one-atom-thick sp^2-bonded carbon atoms densely packed in a hexagon crystal lattice, have rapidly led the science and technology for low-dimensional nanomaterials into a 2D age.[1−3] Recently, the research enthusiasm on 2D materials has largely extended beyond graphene[4] and promoted the rise of numerous 2D monolayer sheets, including natural hexagonal BN,[4,5] dichalcogenide,[4,6] and tertiary B−C−N[7,8] as well as group IV,[9−12] II−VI,[13−15] and III−V compounds[16−18] metastable monolayers, etc., whose buck analogies are not layered in nature. While the reported 2D sheets show different properties ranging from zero gap semimetals (e.g., graphene) to wide gap insulators (e.g., BN sheet), they have a striking common feature: a hexagonal structure due to dominant sp bonding. In turn, these monolayer sheets are similar in many respects, such as edge morphology, isotropic properties, and symmetry-dependent band gap.[19] Here, we find a novel 2D monolayer with robust stability and distinguished structural and physical properties: a tetragonal monolayer TiC (t-TiC) sheet formed by strong in-plane p−d bonding in conjunction with out-of-plane electronic delocalization. Unlike semimetallic graphene and insulating BN sheet, the t-TiC sheet is a semiconductor with an indirect band gap of ∼0.2 eV and exhibits anisotropic mechanical and electronic properties. This finding opens a window to a new land in 2D material physics beyond the hexagonal framework.

Compared with the hexagon, tetragonal lattice is more familiar in everyday living, such as in coating meshes, pavements, and fences. However, a tetragonal monatomic sheet seems impossible according to the valence electron pair repulsion rule[20] that an atom should prefer a spatial arrangement of multiple bonds with its neighbors. Searching for such a form,
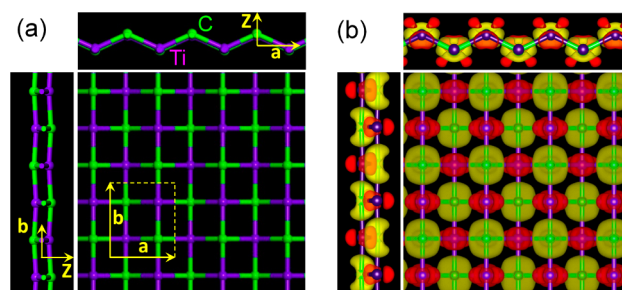
even theoretically, by trial and error encounters often insurmountable difficulties of combinatorics, unless some additional hints are found. Recent theories and experiments[21−23] showed that transition-metal atoms can be firmly embedded into defective graphene sheet. In particular, Ti atom is the most perfect metal with the highest binding energy to fill up the double vacancies by four strong coplanar Ti−C bonds,[21] attributed to the same valence electron number as carbon and its moderate core size. Coincidently, a C atom with four coplanar bonds to its neighboring atoms, known as planar tetracoordinate carbon, has long been proposed[24−26] and synthesized in metal compound molecules.[27] Thus, it offers the possibility to make up a t-TiC monolayer sheet by combining planar tetracoordinate C and Ti atoms. Following this hint, we have performed intensive first-principles structural search of TiC sheets from hundreds of designed structures with different lattice shapes and constants (see Supporting Information (SI) and Figures S1 and S2), as implemented in VASP code; calculation settings are detailed in SI.

Figure 1a presents the atomic structure of the most stable t-TiC sheet obtained in the structural search. The t-TiC sheet unit cell contains two Ti and two C atoms in a rectangular shape, with lattice constants of *a* and *b* being 3.64 and 4.20 Å, respectively. All the atoms in the sheet bond to four neighboring atoms in almost the same plane, forming moieties akin to planar tetracoordinate C atoms in organic molecules.[25,26] To our knowledge, such a 2D system fully composed by quasiplanar tetracoordinate atoms has never been reported, although the planar tetracoordinate C and
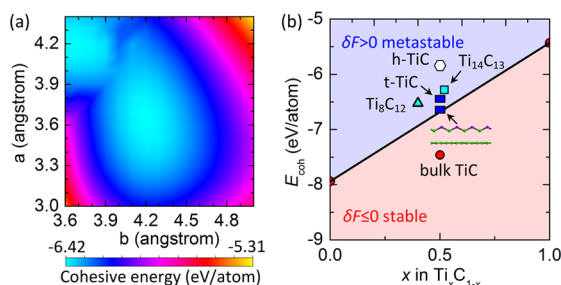
Figure 2. Stability of the t-TiC sheet. (a) Cohesive energy surface calculated with respect to lengths of the lattice vectors **a** and **b**. (b) Cohesive energy for the binary phase composition Ti_xC_{1-x} at different Ti fractions x. Straight line connects cohesive energies of graphene and bulk Ti at $x = 0$ and 1, respectively. Formation energy δF is positive above the line but negative below the line. Inset illustrates the t-TiC sheet supported on a graphene substrate. Experimental structures of the Ti_8C_{12} and $Ti_{14}C_{13}$ clusters are taken from ref 33.

Si atoms have been predicted in 2D B_2C[28] and SiC_2[29] sheets, respectively. It is unique that the t-TiC sheet is buckled into a zigzag line in the view along the vector **b** but exhibits a bilayer structure in the view along the vector **a**. The buckling, measured by the spacing in the bilayer, is 0.88 Å, and the bond angle in the zigzag line is 130°. The length of the Ti−C bond is 2.10 Å along vector **b** but shrinks to 2.02 Å along vector **a**, all remarkably shorter than 2.16 Å in bulk TiC. This buckling structure endows the t-TiC sheet with anisotropic mechanical properties; it behaves very rigid against deformation along the vector **b** as the relative Young's modulus is up to 1.55 TPa Å, about a half of graphene, but becomes over 3× softer along the vector **a**, being reduced to 0.45 TPa Å due to the zigzag buckling feature along this direction. The Poisson ratio is 0.11 and independent of the orientation.

The stability of the t-TiC sheet can first be understood by analyzing its deformation electron density,[30] which reveals electron transfer from the Ti to C atom as shown in Figure 1b. Bader analysis shows a charge transfer of 1.6 e from each Ti atom. The transferred electrons, especially from the Ti $3d_{z^2}$ state, are delocalized around the four Ti−C bonds. Meanwhile, the $2p_z$ state of the C atoms is also found to partially deplete and delocalize over the four Ti−C bonds. The delocalization in the $2p_z$ and $3d_{z^2}$ states is crucial to stabilizing the quasiplanar tetracoordinate atoms, because it not only attenuates atomic activity in forming out-of-plane bonds but also strengthens in-plane Ti−C bonds.

Figure 2a presents the surface of cohesive energy of the t-TiC sheet with respect to variations in the set of lattice constants (a, b). The cohesive energy is found to have a single minimum at (a, b) = (3.64, 4.20) or (4.20, 3.64), attesting that the t-TiC sheet is indeed geometrically stable. The minimum cohesive energy is −6.44 eV/atom, distinctly lower than −5.85 eV/atom for a low-bucked hexagonal TiC sheet (h-TiC). So the TiC sheet prefers a tetragonal lattice rather than the hexagonal one as the BN, SiC, and ZnO monolayer sheets adopt. To further evaluate the relative stability, we define a molar formation energy δF for a composition Ti_xC_{1-x} as[31]

$$\delta F(x) = E_{coh}(x) - x\mu_{Ti} - (1-x)\mu_C \qquad (1)$$

where $E_{coh}(x)$ is the cohesive energy of the system and μ_{Ti} and μ_C are the chemical potentials of the Ti and C atoms, respectively, and depends on the environmental conditions. Then the relative stability of the Ti−C binary structures can be easily measured by
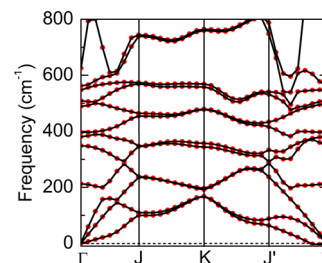

Figure 3. Phonon band dispersion of the t-TiC sheet calculated by linear response theory.

comparing the altitude δF of each $E_{coh}(x)$ point from the line connecting the μ_C at $x = 0$ and μ_{Ti} at $x = 1$. A higher δF means weaker stability. Here, we choose μ_C as the cohesive energy in graphene sheet and μ_{Ti} as that in bulk Ti. Figure 2b plots E_{coh} of TiC sheets and some typical Ti_xC_{1-x} structures. Bulk TiC is shown to be thermodynamically stable as the corresponding E_{coh} is well below the straight line with a negative δF of −0.78 eV. In contrast, the remaining Ti_xC_{1-x} structures with positive δF above this line are metastable. However, δF for the t-TiC sheet is only 0.24 eV, significantly lower than 0.41 eV for the cage-like Ti_8C_{12} and 0.35 eV for the cubic $Ti_{14}C_{13}$ cluster,[32,33] both of which have been experimentally synthesized in gas phase. In particular, when the t-TiC sheet is supported on a graphene sheet by the van der Waals interaction, δF is further reduced to 0.03 eV, which renders the sheet being almost thermodynamically favorable. Therefore, a substrate with suitable interaction may turn the t-TiC sheet into thermodynamically stable and hence facilitate its synthesis.

The stability of the t-TiC sheet is also confirmed by the phonon dispersion curves shown in Figure 3, where appreciable imaginary phonon mode is tiny. So the t-TiC sheet is kinetically stable. The highest frequency of the t-TiC sheet reaches up to 810 cm^{-1}, higher than the highest frequency of 580 cm^{-1} in silicene[9] and 650 cm^{-1} in ZnO sheet, indicative of robust Ti−C bonds in the t-TiC sheet. To further test the thermodynamic stability, we carry out ab initio molecular dynamics simulations. To approach the true stability, we adopt a relatively large supercell consisting of 4×5 repeated units. Simulations of the t-TiC sheet at temperatures of 1500, 2000, and 2500 K show that its structure does not disrupt throughout a 10 ps dynamical simulation up to 2000 K but melts at 2500 K (Figure S3), suggesting high thermal stability of the t-TiC sheet. We also test other metal carbide monolayer sheets, such as VC and ZrC, but find far lower stability than the t-TiC sheet.

Considering the high stability, it is natural to wonder how the t-TiC sheet can be synthesized in experiments. Here, we propose growing the t-TiC sheet on substrates by CVD method, similar to growing graphene on metal surfaces.[34] Since the lattice structure is very different from graphene, it is vital to choose a suitable substrate, which can act as planar catalyst and also should have a good lattice match with the t-TiC sheet. Through a series of test calculations, we find that the NiO(001) surface can well serve this purpose. On NiO(001), the nucleation energy of planar t-TiC nucleus is sharply reduced to be lower than that of the 3D one by over 1 eV within a wide range of sizes (Figure S4). Since δF of the TiC sheet can be reduced by increasing μ_{Ti} and μ_C, nucleation of TiC sheet could be further controlled by adjusting the chemical potential difference between product and Ti and C sources. While the whole nucleation profile with detailed atomic resolution for both 2D and 3D TiC can not be afforded here, these results have pointed to a viable route toward synthesizing
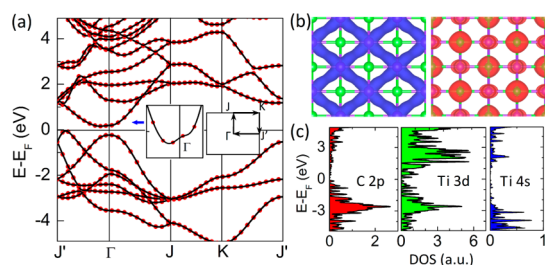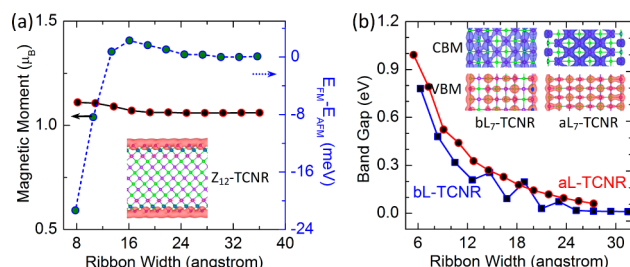
Figure 4. Electronic structure of the t-TiC sheet. (a) HSE06 band structure. Left inset illustrates the minimum band near the Γ point and the right shows the Brillouin zone. (b) Isosurface (0.1 e/Å^3) of partial charge densities of the CBM (left) and VBM (right). (c) Orbit-projected density of states for the C and Ti atoms of the sheet.

Figure 5. Electronic and magnetic properties of TCNRs. (a) Local magnetic moment on each edge Ti atom and the energy difference E_{FM} − E_{AFM} in the Ti-terminated Z-TCNRs as functions of ribbon width. Inset illustrates atomic structure and magnetization density of the Z_{12}-TCNR; red and blue isosurfaces (0.02 e/Å^3) represent the down- and up-spins, respectively. (b) Band gaps of aL- and bL-TCNRs as functions of ribbon width. Insets depict charge density distribution of the CBM and VBM for the (left) bL$_7$- and (right) aL$_7$-TCNRs, respectively.

the TiC sheet with current experimental technology. It is found that any sized Ti aggregation is highly unfavorable in the t-TiC sheet (Figure S5), which further promises fabrication of the sheet given its robust stability over other 2D TiC structures.

If the t-TiC sheet were synthesized, one should wonder whether the 2D sheet possesses novel properties. To this end, we calculate the electronic band structures of the t-TiC sheet as shown in Figure 4a. As the semilocal functional underestimates the band gap for most of the insulators, while the case is greatly improved by using the hybrid functional developed by Heyd, Scuseria, and Ernzerhof (HSE06),[35] we focus on the HSE06 results. Interestingly, the t-TiC sheet is a semiconductor with an indirect band gap of 0.21 eV, in sharp contrast to the semimetallic graphene and insulating BN sheet. Electronic orbital analysis manifests that the conduction band minimum (CBM) near the Γ point (Figure 4a inset) is from the Ti 3d$_{xy}$ state, while valence band maximum (VBM) on the line from Γ to J′ is from the mixed Ti 3d$_{z^2}$–C 2p$_z$ states, as illustrated by the charge density distributions in Figure 4b. What is special here is that the near-gap bands on two sides of the VBM and CBM are not mirror symmetric. Band slope and curvatures are −0.13 eVÅ and 26 eVÅ^2 on the left side of the CBM and 0.26 eVÅ and 15.00 eVÅ^2 on the right side. Corresponding values become 0.94 eVÅ and 176.77 eVÅ^2 on the left side of the VBM and −0.16 eVÅ and 99.78 eVÅ^2 on the right side. Differences in band slopes and curvatures around CBM and VBM suggest direction-dependent electronic properties in the t-TiC sheet. This is attributed to the rectangular symmetry that makes CBM and VBM deviated from high symmetry points, thereby leading to different symmetry dependences of the corresponding bands along the k_x and k_y directions.

To obtain deeper insight into the electronic structure of the TiC sheet, we analyze the orbital-projected atomic density of states in Figure 4c. C 2p and Ti 3d states are mainly distributed in the energy window of 1−4 eV below the VBM and show exact electronic resonance, revealing a strong hybridization between them. In contrast, most weight of the C 2p state mismatches with the distribution of Ti 4s state, saying a much weaker s−p bonding. Therefore, in the t-TiC sheet the bonding states are dominantly contributed by C 2p−Ti 3d hybridization. The prevalent p−d hybridization avails the tetracoordinate bond structure of each atom in the sheet in light of the in-plane orbit symmetries. This hybridization hence favors the formation of a tetragonal lattice. In addition, while the buckling structure slightly raises the energy of in-plane bonding states, it mixes the in- and out-of-plane states and particularly enhances hybridization between the z-oriented orbits on Ti and C atoms (Figure S6), thereby lowering the energy of the z-oriented orbits away

from the Fermi level to open a band gap in the sheet. If the sheet were forced into a pure plane, the band gap will be closed by the C 2p$_z$- and Ti 3d$_{z^2}$-derived bands crossing Fermi level.

For a 2D material, its 1D derivatives always play an important role to deliver its potential into practical applications. In what follows, the electronic properties of the TiC nanoribbons are investigated. We mainly consider three types of nanoribbons with edges along three special crystallographic orientations. The first type is fabricated by tailoring the sheet along the **a** vector, the second along the **b** vector, and the third along the **a**+**b** vector. We denote the nanoribbon tailored along the **a**+**b** vector as zigzag-edged t-TiC nanoribbon (Z-TCNR) and the nanoribbons along the **a** and **b** vectors respectively as a- and b-oriented linear-edged t-TiC ribbons (aL- and bL-TCNR), just like the zigzag and armchair graphene nanoribbons, respectively. For ease of discussion, we use notation Z$_n$-TCNR to describe a Z-TCNR having n Ti−C bonds in the zigzag atomic chain across the ribbon width and use L$_n$-TCNR to describe a L-TCNR whose width consists of n Ti−C bonds, as illustrated by optimized structures of Z$_{12}$-TCNR as well as aL$_7$- and bL$_7$-TCNRs shown in Figure 5 insets, respectively. Considering the computational expense, we use GGA functional for calculating the TCNRs.

Our results show that all the Ti-terminated Z$_n$-TCNRs are magnetic metals, while all the C-terminated Z$_n$-TCNRs are nonmagnetic metals. In Ti-terminated Z$_{12}$-TCNR, polarized electron spins are dominantly contributed by the edge Ti atoms as shown in Figure 5a insets. The magnetic moment on each edge C atom is ∼1.1 μ_B, and total moment amounts to 2.8 μ_B per supercell. Z-TCNR magnetism stems from d-orbit dangling bond states on the edge Ti atoms, and the edge spins can be quenched by, e.g., hydrogen passivation. As a result, both local and total moments hardly change with increasing ribbon width. However, magnetic ordering in Z-TCNR strongly depends on the ribbon width. Coupling of polarized spins on two opposite edges is ferromagnetic in Z-TCNR with width <10 Å but rapidly changes to antiferromagnetic in wider ribbons. This is because a narrow Z-TCNR allows a substantial overlap of wave functions of localized dangling bond states at the two edges and therefore promotes a ferromagnetic coupling between edge spin states, akin to the magnetic coupling mechanism in semiconductors.[36] With increasing ribbon width, such overlap decays promptly to decouple interedge interaction of polarized spins, so energy difference between ferromagnetic and antiferromagnetic states in wide Z-TCNRs approaches zero (∼0.1 meV), rendering them a paramagnetic metal.

In contrast, both aL- and bL-TCNRs are nonmagnetic semiconductors. The aL-TCNR has an indirect band gap, and its band structure can be obtained just by folding the bands of the sheet along Γ to J′, which is parallel to vector **a**; whereas the bL-TCNR has a direct band gap, and its band structure resembles the bands of the 2D sheet along the Γ to J (Figure S7), just in the direction of vector **b**. Indeed, the CBM and VBM charge densities in both L-TCNRs types are similar to those in the t-TiC sheet (Figure 5b insets). Owing to quantum confinement effect, aL- and bL-TCNRs band gaps decrease with increasing ribbon width and converge to the t-TiC sheet value. What is special is that the variation of band gap in the bL_n-TCNRs exhibits an even−odd oscillation with increasing n. This oscillation disappears when the ribbon width is <12 Å, possibly due to enhanced edge effect that dominates the electronic properties of narrow L-TCNRs. The variety of properties in nanoribbons will further enrich the t-TiC sheet applications; e.g., the semi-conducting L-TCNRs can directly serve as electronic components in transistors and also in optical devices with variable light emission, while magnetic Z-TCNRs are promising for applications in spin-polarized electronic transport.

In conclusion, we have shown via statics and dynamics ab initio calculations that 2D tetragonal TiC sheet formed by strong Ti 3d−C 2p hybridization can be stable up to 2000 K at least in our simulation. The t-TiC sheet is buckled with two adjacent rows of atoms shifted oppositely with respect to the plane, forming microscopic washboard morphology, and each atom in the sheet bonds to four neighboring atoms in a quasiplane. The TiC sheet is a natural 2D semiconductor with an indirect band gap ∼0.2 eV, accompanying strongly anisotropic properties, and even exhibits robust edge magnetism when tailored into nanoribbons. Since similar Ti_3C_2 nanosheets and many other 2D transition-metal carbides have been successively synthesized recently,[37,38] we expect that our t-TiC sheet will come out in laboratory soon in view of its fundamental values and potential applications.

■ ASSOCIATED CONTENT

Ⓢ Supporting Information
Experimental details and characterization data. This material is available free of charge via the Internet at http://pubs.acs.org.

■ AUTHOR INFORMATION

Corresponding Author
chuwazhang@nuaa.edu.cn; wlguo@nuaa.edu.cn
Notes
The authors declare no competing financial interest.

■ ACKNOWLEDGMENTS

■ REFERENCES

(1) Novoselov, K. S.; Geim, A. K.; Morozov, S. V.; Jiang, D.; Katsnelson, M. I.; Grigorieva, I. V.; Dubonos, S. V.; Firsov, A. A. *Nature* **2005**, *438*, 197.

(2) Geim, A. K.; Novoselov, K. S. *Nat. Mater.* **2007**, *6*, 183.

(3) Castro Neto, A. H.; Guinea, F.; Peres, N. M. R.; Novoselov, K. S.; Geim, A. K. *Rev. Mod. Phys.* **2009**, *81*, 109.

(4) Novoselov, K. S.; Jiang, D.; Schedin, F.; Booth, T. J. *Proc. Natl. Acad. Sci. U.S.A.* **2005**, *102*, 10451.

(5) Jin, C.; Lin, F.; Suenaga, K.; Iijima, S. *Phys. Rev. Lett.* **2009**, *102*, 195505.

(6) Joensen, P.; Frindt, R. F.; Morrison, S. R. *Mater. Res. Bull.* **1986**, *21*, 457.

(7) Ci, L.; Song, L.; Jin, C.; Jariwala, D.; Wu, D.; Li, Y.; Srivastava, A.; Wang, Z. F.; Liu, F.; Ajayan, P. M. *Nat. Mater.* **2010**, *9*, 430.

(8) Du, A.; Sanvito, S.; Smith, S. C. *Phys. Rev. Lett.* **2012**, *108*, 197207.

(9) Cahangirov, S.; Topsakal, M.; Akturk, E.; Sahin, H.; Ciraci, S. *Phys. Rev. Lett.* **2009**, *102*, 236804.

(10) Padova, P. D.; Quaresima, C.; Ottaviani, C.; Sheverdyaeva, P. M.; Moras, P.; Carbone, C.; Topwal, D.; Olivieri, B.; Kara, A.; Oughaddou, H.; Aufray, B.; Lay, G. L. *Appl. Phys. Lett.* **2010**, *96*, 261905.

(11) Feng, B.; Ding, Z.; Meng, S.; Yao, Y.; He, X.; Cheng, P.; Chen, L.; Wu, K. *Nano Lett.* **2012**, *12*, 3507.

(12) Miyamoto, Y.; Yu, B. D. *Appl. Phys. Lett.* **2002**, *80*, 586.

(13) Wu, W.; Lu, P.; Zhang, Z.; Guo, W. *ACS Appl. Mater. Interfaces* **2011**, *3*, 4787.

(14) Mendez, A. R. B.; Urıas, F. L.; Terrones, M.; Terrones, H. *Nano Lett.* **2008**, *8*, 1562.

(15) Topsakal, M.; Cahangirov, S.; Bekaroglu, E.; Ciraci, S. *Phys. Rev. B* **2009**, *80*, 235119.

(16) Du, A. J.; Zhu, Z. H.; Chen, Y.; Lu, G. Q.; Smith, S. C. *Chem. Phys. Lett.* **2009**, *469*, 183.

(17) Şahin, H.; Cahangirov, S.; Topsakal, M.; Bekaroglu, E.; Akturk, E.; Senger, R. T.; Ciraci, S. *Phys. Rev. B* **2009**, *80*, 155453.

(18) Li, H.; Dai, J.; Li, J.; Zhang, S.; Zhou, J.; Zhang, L.; Chu, W.; Chen, D.; Zhao, H.; Yang, J.; Wu, Z. *J. Phys. Chem. C* **2010**, *114*, 11390.

(19) Novoselov, K. *Nat. Mater.* **2007**, *6*, 720.

(20) Jolly, W. L. *Modern Inorganic Chemistry*; McGraw-Hill: New York, 1984.

(21) Krasheninnikov, A. V.; Lehtinen, P. O.; Foster, A. S.; Pyykko, P.; Nieminen, R. M. *Phys. Rev. Lett.* **2009**, *102*, 126807.

(22) Wang, H.; Wang, Q.; Cheng, Y.; Li, K.; Yao, Y.; Zhang, Q.; Dong, C.; Wang, P.; Schwingenschlög, U.; Yang, W.; Zhang, X. X. *Nano Lett.* **2012**, *12*, 141.

(23) Lisenkov, S.; Andriotis, A. N.; Menon, M. *Phys. Rev. Lett.* **2012**, *108*, 187208.

(24) Hoffmann, R.; Alder, R. W.; Wilcox, C. F., Jr. *J. Am. Chem. Soc.* **1970**, *92*, 4992.

(25) Collins, J. B.; Dill, J. D.; Jemmis, E. D.; Apeloig, Y.; Schleyer, P. v. R.; Seeger, R.; Pople, J. A. *J. Am. Chem. Soc.* **1976**, *98*, 5419.

(26) Pei, Y.; An, W.; Ito, K.; Schleyer, P. R.; Zeng, X. C. *J. Am. Chem. Soc.* **2008**, *130*, 10394.

(27) Cotton, F. A.; Millar, M. *J. Am. Chem. Soc.* **1977**, *99*, 7886.

(28) Wu, X.; Pei, Y.; Zeng, X. C. *Nano Lett.* **2009**, *9*, 1577.

(29) Li, Y.; Zhou, Z.; Chen, Z. *J. Am. Chem. Soc.* **2011**, *133*, 900.

(30) Deformation electron density is defined as the t-TiC sheet total charge density subtracting the sum of isolated atoms.

(31) Dumitrică, T.; Hua, M.; Yakobson, B. I. *Phys. Rev. B* **2004**, *70*, 241303.

(32) Guo, B. C.; Kerns, K. P.; Castleman, A. W., Jr. *Science* **1992**, *255*, 1411.

(33) vanHeijnsbergen, D.; vonHelden, G.; Duncan, M. A.; vanRoij, A. J. A.; Meijer, G. *Phys. Rev. Lett.* **1999**, *83*, 4983.

(34) Gao, J.; Yip, J.; Zhao, J.; Yakobson, B. I.; Ding, F. *J. Am. Chem. Soc.* **2011**, *133*, 5009.

(35) Heyd, J.; Scuseria, G. E.; Ernzerhof, M. *J. Chem. Phys.* **2003**, *118*, 8207.

(36) Dalpian, G. M.; Wei, S. H.; Gong, X. G.; Da Silva, A. J. R.; Fazzio, A. *Solid State Commun.* **2006**, *138*, 353.

(37) Naguib, M.; Kurtoglu, M.; Presser, V.; Lu, J.; Niu, J.; Heon, M.; Hultman, L.; Gogotsi, Y. *Adv. Mater.* **2011**, *23*, 4248.

(38) Naguib, M.; Mashtalir, O.; Carle, J.; Presser, V.; Lu, J.; Hultman, L.; Gogotsi, Y.; Barsoum, M. W. *ACS Nano* **2012**, *6*, 1322.